Distinction between shadow and edge effects in heavy-ion elastic angular distributions

R. da Silveira[1] and Ch. Leclercq-Willain[2]
[1]*Groupe de Physique Théorique, Institut de Physique Nucléaire, F-91406, Orsay Cedex, France*
[2]*Physique Nucléaire Théorique et Mathématique, CP229-Universite Libre, de Bruxelles, B-1050 Bruxelles, Belgium*

(Received 8 June 2004; published 7 October 2004)

We propose a model independent method which allows us to distinguish between shadow and edge or surface effects in the angular distributions of heavy-ion elastic scattering, showing regular patterns of marked oscillations. The method is illustrated with a few experimental results where this undulatory behavior is present.

DOI: 10.1103/PhysRevC.70.044604 PACS number(s): 25.70.Bc

I. INTRODUCTION

The angular distributions of heavy-ion elastic scattering often show a regular pattern of marked oscillations (r.p.m.o.) peaked forward and also backward, with angular spacing between successive maxima almost constant and accurately given by

$$\delta\theta = \pi/l_g, \tag{1}$$

where l_g is the grazing or peripheral angular momentum [1]. As is well known, these r.p.m.o. can be produced by two quite different mechanisms: diffraction due to a shadow effect, or scattering arising from surface or edge effects. In the forward direction the distinction between shadow and edge effects from quite similar r.p.m.o. is often a source of misinterpretation. So, the aim of the present paper is to propose a model-independent procedure, based on an extension [2] of Babinet's principle, allowing one to decide which of these mechanisms is responsible for the observed scattering patterns.

II. THEORY

Before going into the details of the method, let us first consider the physical conditions under which the r.p.m.o. are observed. If the Sommerfeld parameter is such that $\eta = Z_1 Z_2 e^2/\hbar v \lesssim 1$ and the grazing angle $\theta_g \approx 2\eta/l_g \ll 1$, one observes in the near forward direction a r.p.m.o. attributed to a shadow effect due to strong absorption. By optical analogy this is often referred to as Fraunhofer diffraction (Fig. 1). For $\eta \gg 1, \theta_g \lesssim 1$, a r.p.m.o. can occur in both the forward [3,4] and the backward directions [5–7]. These are called edge, surface, or glory scattering [8,9] (Figs. 2 and 3).

These effects cannot be observed directly in the forward direction, since they are completely hidden by Coulomb scattering. However, several methods [3,10,11] allow us to extract from the experimental data the modulus of the so-called "nuclear amplitude" $f_n(\theta)$ defined through

$$f(\theta) = f_c(\theta) + f_n(\theta), \tag{2}$$

where $f(\theta)$ and $f_c(\theta)$ are, respectively, the total and the Coulomb amplitudes (see details below). The modulus $|f_n(\theta)|$ so obtained [10,11] exhibits a r.p.m.o. (Figs. 4 and 5).

In order to distinguish between shadow and edge or surface effects, we will invoke, by optical analogy, an extension [2] of Babinet's principle, which can be formulated as follows: the Fraunhofer diffraction pattern produced by an opaque screen and the one produced by a narrow slit having the shape of its edge, oscillate "180° out of phase," or in quadrature, i.e., the maxima of one pattern coincides with the minima of the other and vice versa. To verify that this phase rule also holds in heavy-ion scattering, we begin with the expression of the elastic amplitude $f(\theta)$, separated as in Eq. (2) into a Coulomb and a nuclear part,

$$f(\theta) = f_c(\theta) + (1/2ik)\sum_{l=0}^{\infty}(2l+1)e^{2i\sigma_l}(S_{nl}-1)P_l(\cos\,\theta), \tag{3}$$

where σ_l is the Coulomb phase shift and S_{nl} is related to the partial wave amplitude S_l through

$$S_l = S_{nl}e^{2i\sigma_l}.$$

If $\eta \lesssim 1$, the Coulomb field has little effect on the elastic scattering and may be neglected in first order. Further, assuming strong absorption with a sharp cutoff, such that

$$S_{nl} = 0, \quad l < l_g \quad \text{and} \quad S_{nl} = 1, \quad l \geqslant l_g, \tag{4}$$

and using for the $P_l(\cos\,\theta)$ the small-angle approximation

$$P_l(\cos\,\theta) \approx J_0(l\theta), \quad l \gg 1, \tag{5}$$

one obtains the well-known formula

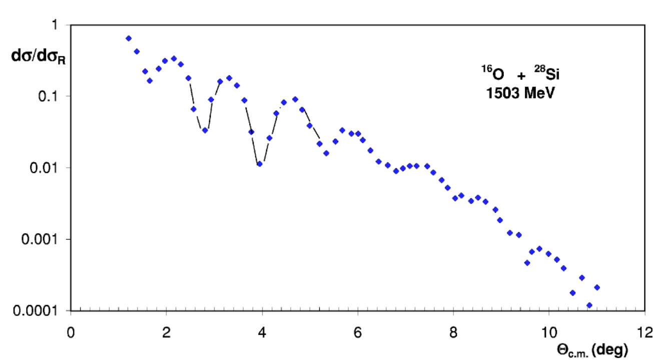

FIG. 1. Angular distribution of elastic scattering of ^{16}O on ^{28}Si at $E_L = 1503$ MeV, from Ref. [13]. The data are linked to guide the eyes.

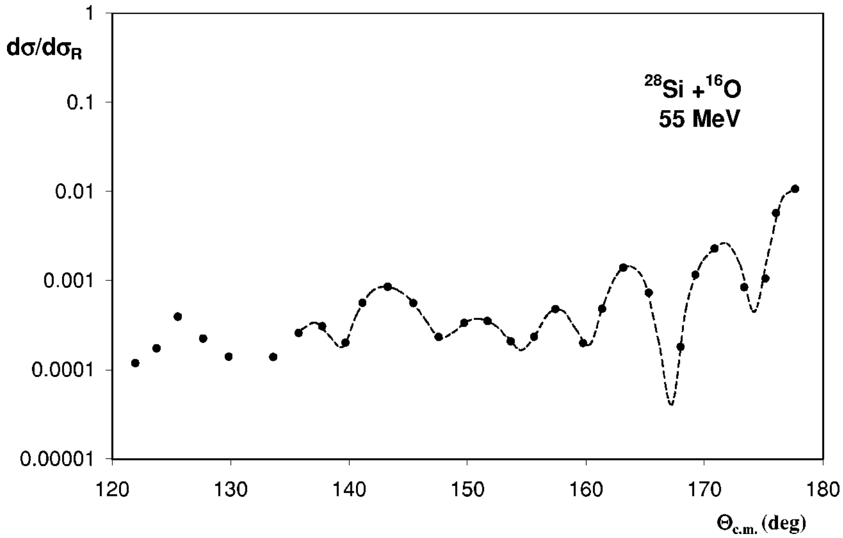

FIG. 2. Same as for Fig. 1, for the elastic scattering of ^{16}O on ^{28}Si at E_L=55 MeV, from Ref. [6].

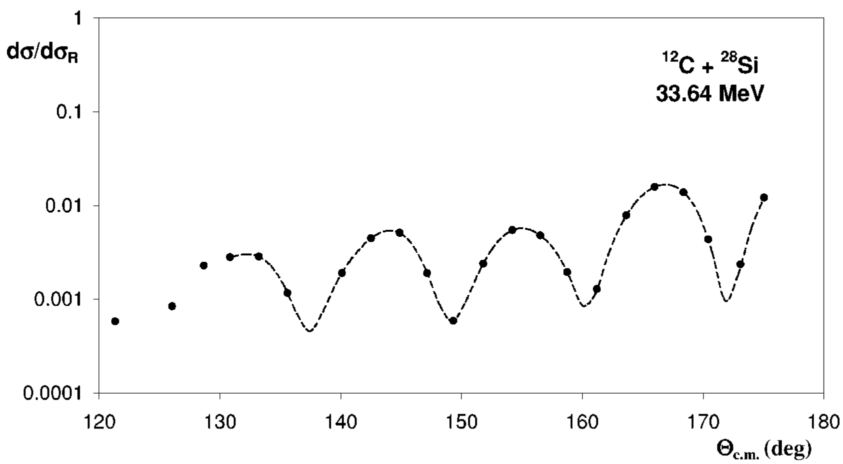

FIG. 3. Same as for Fig. 1 for the elastic scattering of ^{12}C on ^{28}Si at E_L=33.64 MeV, from Ref. [7].

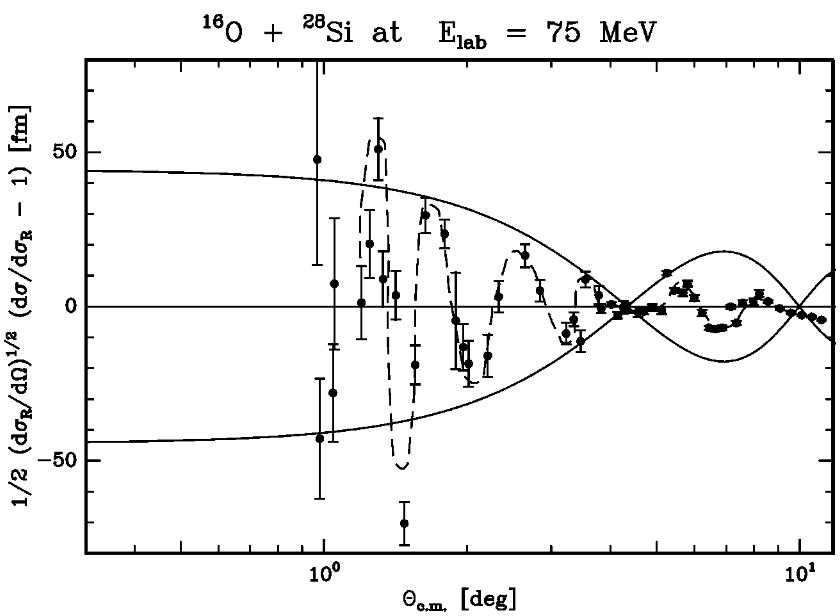

FIG. 4. Elastic scattering of ^{16}O on ^{28}Si at E_L=75 MeV. The points plot $\frac{1}{2}(d\sigma_R/d\Omega)^{1/2}$ $(d\sigma/d\sigma_R-1)$ as a function of θ (log scale), using for $d\sigma/d\Omega$ the experimental data. The broken lines have been drawn through the points to localize the extrema of the fast oscillation. The solid line has been obtained by searching the value of $|f_n(0)|$ such that $|f_n(0)|\,|J_0(l_g\,\theta)|$ envelopes the rapid oscillations (see text).

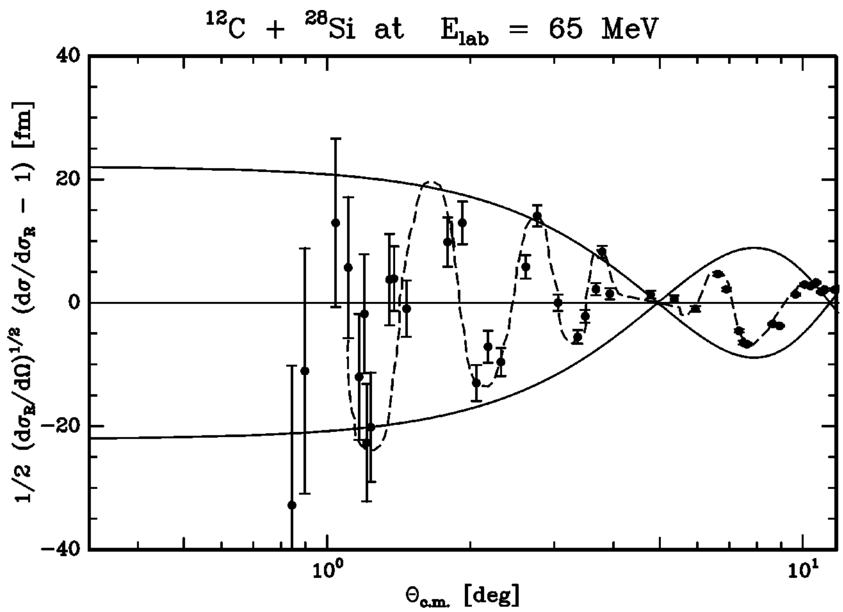

FIG. 5. Same as for Fig. 4 for the elastic scattering of ^{12}C on ^{28}Si at E_L=65 MeV.

$$|f(\theta)|^2 \approx (l_g R)^2 [J_1(l_g\ \theta)/l_g\ \theta]^2. \tag{6}$$

The expression (6) gives the intensity of the Fraunhofer diffraction pattern produced by an opaque disk of radius $R \approx l_g/k$.

If $n \gg 1$, the Coulomb force can no longer be neglected and the expression for $f_n(\theta)$ becomes, from Eq. (3),

$$f_n(\theta) = -\frac{1}{2ik}\sum_{l=0}^{l=l_g}(2l+1)e^{2i\sigma_l}P_l(\cos\ \theta). \tag{7}$$

An approximate analytical result cannot be obtained from the partial wave l summation in Eq. (7). Rather, we shall use semiclassical arguments which provide some physical insight into the scattering mechanism described by $f_n(\theta)$.

At first, one easily verifies that $-f_n(\theta)$ is the scattering amplitude of a Coulomb wave scattered by an opaque screen in which is cut a circular hole with the same radius as the disk [12]. This is illustrated in Fig. 6, in a classical picture, where we have drawn the Rutherford trajectories for the scattering of ^{16}O on ^{28}Si (E_L=75 MeV). As seen, trajectories with the smallest l's values are scattered backward while those with $l > l_g = 32$ are reflected or absorbed. So the only trajectories scattered forward are those passing near the edge of the hole. In the language of wave mechanics, this means that the only contributions to $f_n(\theta)$ in the forward direction come from waves scattered from the edge of the aperture.

The amplitude of these scattered edge waves behaves like $J_0(l_g\theta)$ and one can write approximately

$$|f_n(\theta)|^2 \approx C\ J_0^2(l_g\theta), \tag{8}$$

where C is a constant.

Figure 7 shows, for ^{16}O+^{28}Si (75 MeV), a comparison between the curve obtained from the numerical evaluation of $|f_n(\theta)|^2$ with $f_n(\theta)$ as given by expression (7), with that obtained from the approximate expression (8) putting $C = |f_n(0)|^2$, plotted versus $x = l_g\ \theta$. As seen, the two curves remain close to each other even for not to small values of x.

The same angular dependence as that given by the expression (8) is obtained [8] for the scattering cross section arising from surface waves produced by the real part of the nucleus-nucleus optical potential. This is the so-called glory scattering, a refractive effect which can manifest itself in both the

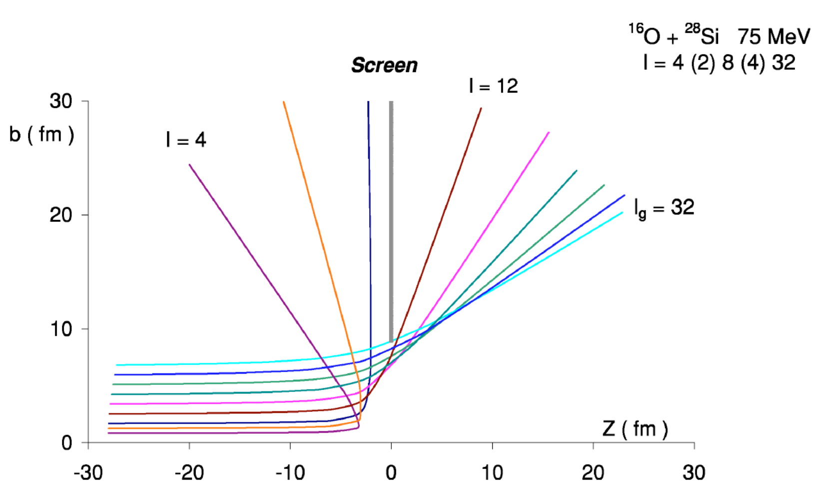

FIG. 6. (Color online) The Rutherford trajectories corresponding to the Coulomb scattering of ^{16}O on ^{28}Si, E_L=75 MeV. The trajectories are collimated by a circular hole cut on an opaque screen. As seen, the only trajectories scattered forward are those passing near the edge of the hole (see text).

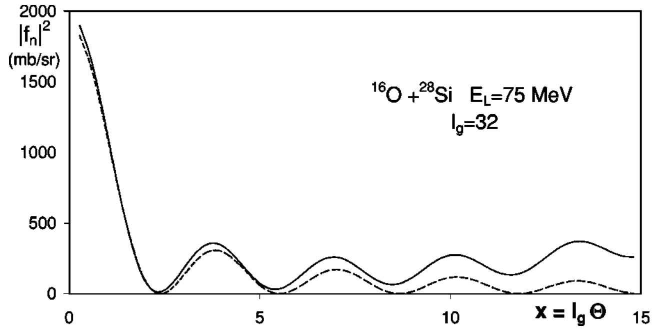

FIG. 7. Comparison between the numerical evaluation of $|f_n(\theta)|^2$ with $f_n(\theta)$ as given by Eq. (7) (full curve) and that of the approximate expression (8) (broken curve).

forward and the backward directions with the same oscillatory behavior [5,8,9]. To go further, one remarks that the location of the extrema of the oscillatory patterns as given by the formulas (6) and (8) depends only on the momentum transfer

$$q = l_g\ \theta. \tag{9}$$

Further, beyond their first maximum, the Bessel functions approach quickly their asymptotic form

$$J_n^2(q) \sim (2\pi/q)\ \cos^2\left(q - n\frac{\pi}{2} - \frac{\pi}{4}\right), \quad n = 0,1. \tag{10}$$

One sees that except around $\theta \sim 0$, $(\pi-\theta) \sim 0$, the r.p.m.o. produced by shadow scattering $(n=1)$ and that produced by edge or surface scattering $(n=0)$ oscillate "180° out of phase," i.e., in quadrature, in accordance with the extension of Babinet's principle. Furthermore, this phase rule should be apparent if the experimental oscillatory patterns are plotted

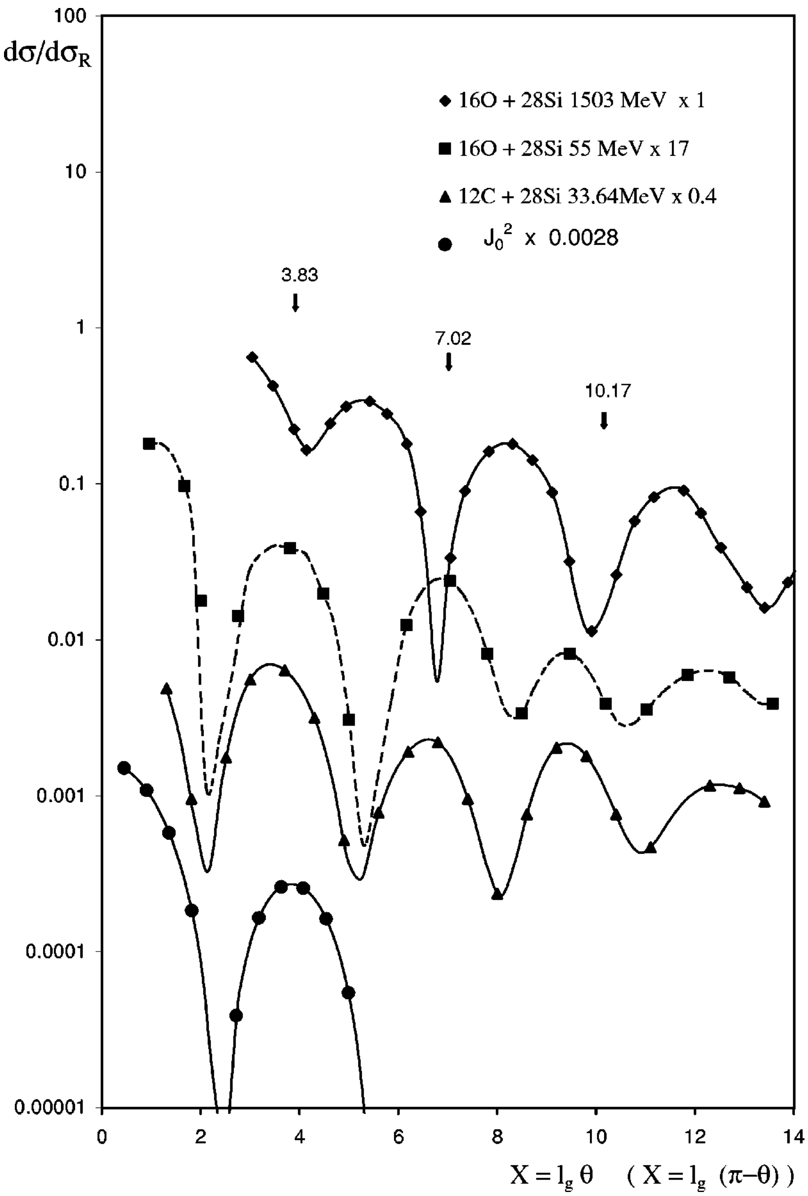

FIG. 8. The points are the experimental data shown in Figs. 1–3 plotted versus the variable $x = l_g\ \theta$ for forward scattering or $x = l_g(\pi-\theta)$ for backward scattering. The data are linked to guide the eyes. The lower curve is a plot of the expression $J_0^2(x)$ in the domain where it reproduces the angular dependence of the evelopes shown in Figs. 4 and 5 (see text). The location of the three first zeros of $J_1^2(x)$ are indicated. A striking feature of these plots is the experimental evidence for the "180° out of phase" rule between the oscillation due to shadow effects (upper curve) and those due to surface effects (lower curves).

versus the variable $x = l_g\ \theta$. This result will be used in the next paragraph to distinguish, in the experimental data, shadow effects from edge or surface effects.

III. EXPERIMENTAL EVIDENCE FOR THE "180° OUT OF PHASE" RULE

Figures 1–3 show examples of angular distributions exhibiting regular patterns of marked oscillations. Figure 1 is a plot of $d\sigma/d\sigma_R$ [13] for the scattering of ^{16}O on ^{28}Si, $E_L = 1503$ MeV, $\eta = 1.82$. The l_g value can be obtained from $\delta\ \theta$ expression (1) measured between successive maxima. One has $\delta\ \theta \sim 1.25°$ and $l_g \sim 1.44$. Figures 2 and 3 are examples of r.p.m.o. peaked backward. For $^{16}\mathrm{O} + {}^{28}\mathrm{Si}$, $E_L = 55$ MeV [6], $\eta = 9.51$, one has $\delta\ \theta \sim 7.3°$, $l_g \sim 25$. For $^{12}\mathrm{C} + {}^{28}\mathrm{Si}$, $E_L = 33.64$ MeV [7], $\eta = 7.9$, $\delta\ \theta \sim 11.7°$, $l_g \sim 15$. When searching for the occurrence of surface effects in the forward direction, one should have in mind that for $\eta \gg 1$ these effects will be hidden by Coulomb scattering. However, a simple method [11] allows us to extract $|f_n(\theta)|$ from the measured scattering cross section $d\sigma/d\Omega$, providing sufficiently accurate experimental data are available at very small angles. It has been shown [11] that if $\eta \gg 1$ and $\theta \ll \theta_g$, the following relation holds:

$$\frac{1}{2}\left(\frac{d\sigma_R}{d\Omega}\right)^{1/2}\left(\frac{d\sigma}{d\sigma_R} - 1\right) = |f_n(\theta)|\cos(\varphi_n - \varphi_c), \qquad (11)$$

where $d\sigma_R/d\Omega$ is the Rutherford cross section. $\varphi_c = \pi - 2\eta\ \ln\ (\sin\ \theta/2) + 2\sigma_0$ and φ_n are, respectively, the Coulomb and the nuclear phase. In the near-forward direction the Coulomb phase varies rapidly and therefore the left-hand side of Eq. (11) oscillates with spacing $\delta \sim \pi\theta/\eta$ and envelopes given by $\pm|f_n(\theta)|$. The points in Figs. 4 and 5 are the plots of $1/2\sqrt{d\sigma_R/d\Omega}(d\sigma/d\sigma_R - 1)$, for the scattering of ^{16}O on ^{28}Si ($E_L = 75$ MeV) and ^{12}C on ^{28}Si ($E_L = 55$ MeV) respectively, using for $d\sigma/d\sigma_R$ the experimental data [4]. The broken line has been drawn through the points to localize the extrema of the fast oscillations. The grazing angular momentum l_g can be obtained from the measured ratio $d\sigma/d\sigma_R$ [4] using the "quarter point recipe″ [14,1]. This gives $l_g = 32$ for $^{16}\mathrm{C} + {}^{28}\mathrm{Si}$ and $l_g = 28$ for $^{12}\mathrm{C} + {}^{28}\mathrm{Si}$. With these l_g values, the envelopes of the fast oscillations in Figs. 4 and 5 follow quite well a zero-order Bessel function. This allows us to write

$$|f_n(\theta)|^2 \approx |f_n(0)|^2\ J_0^2(l_g\theta) \qquad (12)$$

with [11] $|f_n(0)| = 43$ fm for $^{16}\mathrm{O} + {}^{28}\mathrm{Si}$ and $|f_n(0)| = 28$ fm for $^{12}\mathrm{C} + {}^{28}\mathrm{Si}$.

Figure 8 displays the experimental data shown in Figs. 1–3 plotted versus the variable $x = l_g\ \theta$ [$x = l_g(\pi - \theta)$ for backward scattering]. The data are linked to guide the eyes. The lower curve is a plot of $J_0^2(x)$ in the x domain where the envelopes in Figs. 4 and 5 have been drawn.

IV. DISCUSSION

Before going into the discussion of Fig. 8, let us first remark that the difference between the location of the extrema of $d\sigma/d\Omega$ and that of the ratio $d\sigma/d\sigma_R$ is negligible when compared with the angular spacing $\delta\ \theta$ as given by the expression (1). Now, concerning the curve $^{16}\mathrm{O} + {}^{28}\mathrm{Si}$ (1503 MeV), one observes that the first three minima of $d\sigma/d\sigma_R$ occur at the zeros $x_1 = 3.83$, $x_2 = 7.02$, $x_3 = 10.17$ of the function $J_1(x)$. So, the data at $E_L = 1503$ MeV should be attributed to Fraunhofer diffraction, i.e., a shadow effect. Concerning the lower curves, one observes for $x < 10$ two striking features:

(i) these curves oscillate in phase with each other,

(ii) they oscillate "180° out of phase," when compared with the curve for shadow scattering.

So, invoking the extension of the Babinet's principle, one concludes that these angular distributions should be interpreted as resulting from

- backward-surface scattering: $^{12}\mathrm{C} + {}^{28}\mathrm{Si}$ (33.6 MeV) and $^{16}\mathrm{O} + {}^{28}\mathrm{Si}$ (55 MeV);
- forward-surface scattering: $^{12}\mathrm{C} + {}^{28}\mathrm{Si}$ (65 MeV) and $^{16}\mathrm{O} + {}^{28}\mathrm{Si}$ (75 MeV).

In view of Fig. 8, the distinction between shadow and edge or surface scattering appears quite clearly. We think that the present results should also be useful when applying the conventional optical model analysis of the elastic scattering. In fact, in many cases, the numerical calculations of $d\sigma/d\Omega$ done with parametrized optical potentials can hardly answer unambiguously the question of what kind of scattering mechanisms is responsible for the particular pattern so obtained.

[1] D. M. Brink, *Semiclassical Methods in Nucleus-Nucleus Scattering* (Cambridge University Press, Cambridge, England, 1985).

[2] R. da Silveira, J. Mod. Opt. **38**, 1349 (1991); Phys. Lett. B **264**, 248 (1991).

[3] A. N. Ostrowski, W. Tiereth, and H. Voit, Phys. Rev. C **44**, 2082 (1991).

[4] T. Yamaya, H. Ishiyama, A. Yamazaki, J. Tojima, M. Katoh, T. Kuzumaki, H. Yahata, K. Suzuki, K. Kotajima, T. Shinozuka, and M. Fujioka, Phys. Lett. B **417**, 7 (1998).

[5] H. C. Bryant and N. Jarmie, Ann. Phys. (N.Y.) **47**, 127 (1968).

[6] P. Braun-Munzinger, G. M. Berkowitz, T. M. Cormier, C. M. Jachcinski, J. W. Harris, J. Barrette, and M. J. Levine, Phys. Rev. Lett. **38**, 944 (1977).

[7] R. Ost, M. R. Clover, R. M. Devries, N. J. A. Rust, R. N. Cherry, and H. E. Gove, *Proceedings of the Symposium on Heavy-Ion Elastic Scattering*, Rochester, 1977.

[8] K. W. Ford and J. A. Wheeler, Ann. Phys. (N.Y.) **7**, 259 (1959).

[9] H. M. Nussenzveig, *Diffraction Effects in Semiclassical Scattering* (Cambridge University Press, Cambridge, England, 1992).

[10] J. Barrette and N. Alamanos, Nucl. Phys. **A441**, 733 (1985).
[11] R. da Silveira, A. Boukour, and Ch. Leclercq-Willain, Eur. Phys. J. A **7**, 503 (2000).
[12] K. R. Greider, Annu. Rev. Nucl. Sci. **15**, 291 (1965).
[13] P. Roussel, N. Alamanos, F. Auger, J. Barrette, B. Berthier, B. Fernandez, L. Papineau, H. Doubre, and W. Mittig, Phys. Rev. Lett. **54**, 1779 (1985).
[14] J. S. Blair, Phys. Rev. **95**, 1218 (1954).